# Supporting Information for

# Photoinduced energy and electron transfers at graphene quantum dot /azobenzene interfaces

Magdalena Kaźmierczak[1], Samuele Giannini[2,3], Silvio Osella[1]*

[1]Chemical and Biological Systems Simulation Lab, Centre of New Technologies, University of Warsaw, Banacha 2C, 02-097 Warsaw, Poland

[2]Laboratory for Chemistry of Novel Materials, University of Mons, 7000 Mons, Belgium.

[3]Present address: Institute of Chemistry of OrganoMetallic Compounds, National Research Council (ICCOM-CNR), I-56124 Pisa, Italy

Email: s.osella@cent.uw.edu.pl

## Excitation energies

**Table S1** Detailed description of excited states for isolated AZO. Energies of each excited states are reported in nm. Oscillator strength is reported in bracket.

| Excited state | *t*AZO | | *c*AZO | |
|---|---|---|---|---|
| | Fold | Open | Fold | Open |
| 1 | 434 (0.00)<br>HOMO-3 → LUMO | 435 (0.00)<br>HOMO-3 → LUMO | 459 (0.06)<br>HOMO-1 → LUMO+1 | 454 (0.05)<br>HOMO-1 → LUMO+1 |
| 2 | 332 (0.57)<br>HOMO-1 → LUMO | 328 (1.15)<br>HOMO-1 → LUMO | 317 (0.23)<br>HOMO → LUMO | 309 (0.33)<br>HOMO → LUMO |
| 3 | 317 (0.07)<br>HOMO → LUMO | 308 (0.17)<br>HOMO → LUMO+1 | 309 (0.03)<br>HOMO → LUMO+2 | 307 (0.08)<br>HOMO → LUMO+2 |
| 4 | 314 (0.46)<br>HOMO → LUMO+1 | 306 (0.19)<br>HOMO → LUMO+1 | 288 (0.30)<br>HOMO-1 → LUMO+1 | 285 (0.29)<br>HOMO-3 → LUMO+1 |
| 5 | 308 (0.08)<br>HOMO → LUMO+2 | 258 (0.01)<br>HOMO-1 → LUMO+4 | 282 (0.03)<br>HOMO → LUMO+1 | 263 (0.08)<br>HOMO-1 → LUMO+3 |
| 6 | 272 (0.02)<br>HOMO-1 → LUMO+1 | 253 (0.00)<br>HOMO → LUMO+3 | 274 (0.03)<br>HOMO-1 → LUMO | 259 (0.05)<br>HOMO-4 → LUMO+1 |
| 7 | 263 (0.02)<br>HOMO-6 → LUMO | 252 (0.00)<br>HOMO-5 → LUMO | 266 (0.06)<br>HOMO-3 → LUMO+1 | 252 (0.00)<br>HOMO → LUMO+5 |
| 8 | 257 (0.01)<br>HOMO-1 → LUMO+3 | 244 (0.01)<br>HOMO → LUMO | 262 (0.01)<br>HOMO-1 → LUMO+3 | 247 (0.00)<br>HOMO-1 → LUMO+3 |
| 9 | 252 (0.01)<br>HOMO →LUMO+4 | 242 (0.32)<br>HOMO-4 → LUMO | 253 (0.00)<br>HOMO → LUMO+5 | 241 (0.39)<br>HOMO-2 → LUMO |
| 10 | 252 (0.03)<br>HOMO-6 → LUMO | 241 (0.15)<br>HOMO-4 → LUMO | 249 (0.01)<br>HOMO-1 → LUMO+6 | 241 (0.03)<br>HOMO-5 → LUMO |

| | | | | |
|---|---|---|---|---|
| 11 | 247 (0.24)<br>HOMO-2 → LUMO+1 | 240 (0.00)<br>HOMO-7 → LUMO+1 | 246 (0.22)<br>HOMO-2 → LUMO | 229 (0.00)<br>HOMO → LUMO+1 |
| 12 | 246 (0.00)<br>HOMO-6 →LUMO+1 | 225 (0.00)<br>HOMO-1 → LUMO+1 | 244 (0.02)<br>HOMO-5 → LUMO | 228 (0.00)<br>HOMO-1 → LUMO |
| 13 | 242 (0.01)<br>HOMO-4 → LUMO | 220 (0.15)<br>HOMO-6 → LUMO | 233 (0.03)<br>HOMO-2 → LUMO+1 | 224 (0.20)<br>HOMO-6 → LUMO+1 |
| 14 | 236 (0.00)<br>HOMO-3 → LUMO+1 | 217 (0.00)<br>HOMO-2 → LUMO+3 | 228 (0.03)<br>HOMO → LUMO+4 | 222 (0.10)<br>HOMO-1 → LUMO+4 |
| 15 | 225 (0.20)<br>HOMO-1 → LUMO+2 | 215 (0.21)<br>HOMO-9 → LUMO+6 | 227 (0.19)<br>HOMO-5 → LUMO+1 | 217 (0.01)<br>HOMO-2 → LUMO+5 |
| 16 | 224 (0.01)<br>HOMO-9 → LUMO+6 | 215 (0.74)<br>HOMO-2 → LUMO+2 | 226 (0.06)<br>HOMO → LUMO+4 | 215 (0.94)<br>HOMO-2 → LUMO+2 |
| 17 | 222 (0.04)<br>HOMO → LUMO+4 | 208 (0.19)<br>HOMO-1 → LUMO+4 | 224 (0.01)<br>HOMO-3 → LUMO | 214 (0.05)<br>HOMO-9 → LUMO+8 |
| 18 | 220 (0.13)<br>HOMO-2 → LUMO+2 | 206 (0.01)<br>HOMO → LUMO+7 | 223 (0.00)<br>HOMO → LUMO+4 | 213 (0.01)<br>HOMO-7 → LUMO+2 |
| 19 | 218 (0.13)<br>HOMO-7 → LUMO | 204 (0.01)<br>HOMO-2 → LUMO | 221 (0.01)<br>HOMO → LUMO+3 | 206 (0.02)<br>HOMO → LUMO+7 |
| 20 | 217 (0.07)<br>HOMO-4 → LUMO+1 | 204 (0.01)<br>HOMO-8 → LUMO+1 | 220 (0.03)<br>HOMO → LUMO | 205 (0.05)<br>HOMO-1 → LUMO+9 |

**Internal reorganization energy calculation for interfaces**

When considering the interface consisting of donor and acceptor fragments, one can separately calculate the internal reorganization energy as an average of the backward ($\lambda_{Bw}$) and forward transitions ($\lambda_{Fw}$) as:

- PET

$$\lambda_{Bw} = E(D^* @ D^+) - E(D^* @ D^*) + E(A @ A^-) - E(A @ A) \quad \text{(S1)}$$

$$\lambda_{Fw} = E(D^+ @ D^*) - E(D^+ @ D^+) + E(A^- @ A) - E(A^- @ A^-)$$

- PHT

$$\lambda_{Bw} = E(D @ D^+) - E(D @ D) + E(A^* @ A^-) - E(A^* @ A^*) \quad \text{(S2)}$$

$$\lambda_{Fw} = E(D^+ @ D) - E(D^+ @ D^+) + E(A^- @ A^*) - E(A^- @ A^-)$$

- EET

$$\lambda_{Bw} = E(D^* @ D) - E(D^* @ D^*) + E(A @ A^*) - E(A @ A) \quad \text{(S3)}$$

$$\lambda_{Fw} = E(D @ D^*) - E(D @ D) + E(A^* @ A) - E(A^* @ A^*)$$

where D indicates the donor fragment and A the acceptor fragment in their excited states (i.e., anionic, cation or excitonic states).

**Table S2.** Reorganization energy, coupling, driving force and Marcus rates for the three processes considered in this study, for the AZO molecule isolated.

| | **Process** | **λ [eV]** | **Coupling [eV]** | Involved transitions |
|---|---|---|---|---|
| ***t*AZO** | EET | 0.14 | 0.021 | $D^*_{PYR}$ ($S_3$, $S_4$), $A^*_{AZO}$ ($S_2$) |
| | PET | 0.75 | 0.009 | $D^*_{PYR}$ ($S_3$, $S_4$), $D_{PYR}\rightarrow A_{AZO}$ ($S_8$) |
| | PHT | 0.64 | 0.003 | $A^*_{AZO}$ ($S_2$), $A_{AZO}\rightarrow D_{PYR}$ ($S_8$) |
| ***c*AZO** | EET | 0.24 | 0.010 | $D^*_{PYR}$ ($S_2$), $A^*_{AZO}$ ($S_1$) |
| | PET | 1.26 | 0.010 | $D^*_{PYR}$ ($S_2$), $D_{PYR}\rightarrow A_{AZO}$ ($S_5$) |
| | PHT | 1.24 | 0.003 | $A^*_{AZO}$ ($S_1$), $A_{AZO}\rightarrow D_{PYR}$($S_5$) |

**Photo-induced energy and electron transfer couplings**

The photoinduced interaction between donor and acceptor moieties can essentially be written as the sum of two components: a long-range Coulomb interaction between the transition density of the two moieties/fragments and a short range Dexter-like exchange interaction [1]:

$$V = V_{Coul} + V_{short}$$

The first term resembles a classical interaction between two density distributions. The first term of the dipolar expansion of the density distribution is the dipole moment. Therefore, the Coulomb term can be written as a dipole-dipole interaction which scales as $1/r^3$ as a function of the distance and it is mostly related to the reciprocal orientation of the interacting transition dipoles (leading to the famous Forster-like equation) and the magnitude of the interacting dipoles. As such, the distance dependence is not so strong.

The second term is a Dexter-like exchange and decays exponentially with the distance between the two moieties (thus, much faster than the Coulomb interaction). This second term is more sensitive to the actual orbital shape and specific overlap between the wavefunction two moieties. Usually, it is negligible compared to the first Coulomb term. However, it might be important in the case of the interaction of almost forbidden transition with a small oscillator strength (which nullify the Coulomb interaction).

Importantly, since the diabatization scheme used in this work starts from the adiabatic wavefunction of the full system, it contains both Coulomb and Dexter-like exchange included in the final coupling values. We refer to Ref 1-4 for a deep analysis of the diabatization method used.

**Optimized structure and absorption spectra of the azobenzene moiety**

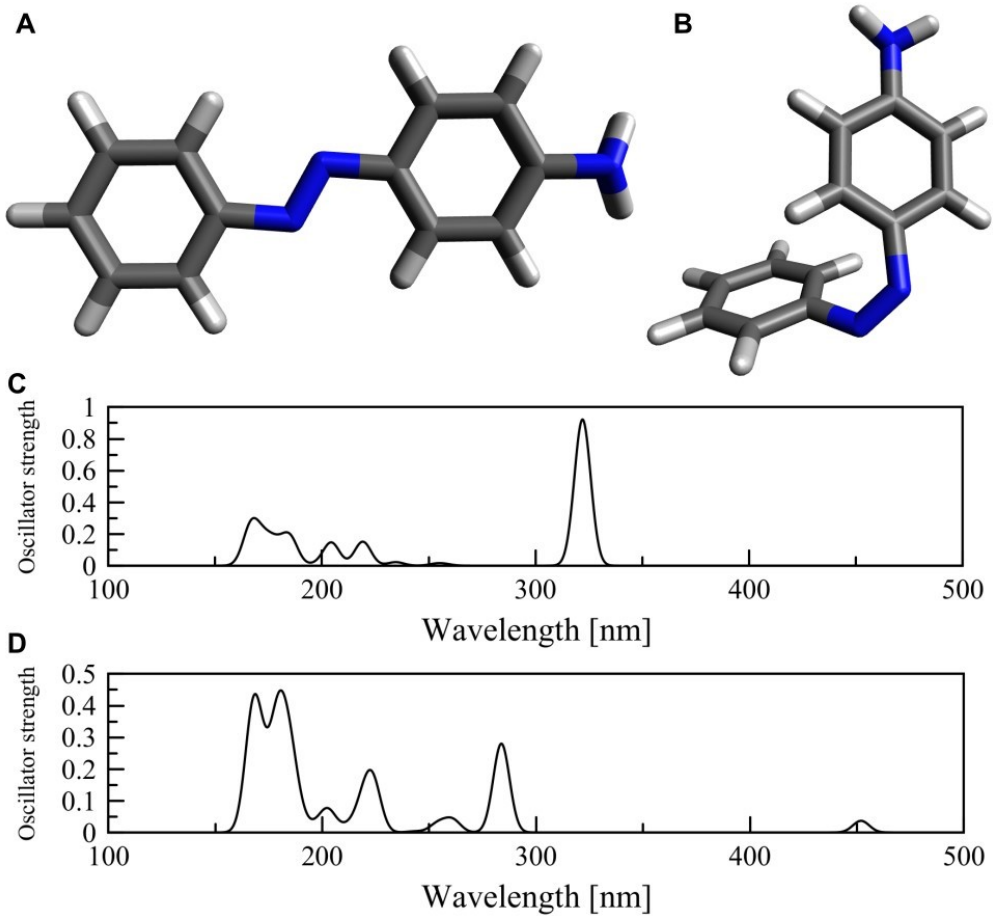


**Figure S1** The structure of $NH_2$-functionalized azobenzene molecules (A-*trans*, B-*cis*), C - UV-Vis spectra for isomer *trans*, D - UV-Vis spectra for isomer *cis*

**Discussion on the open-AZO conformation**

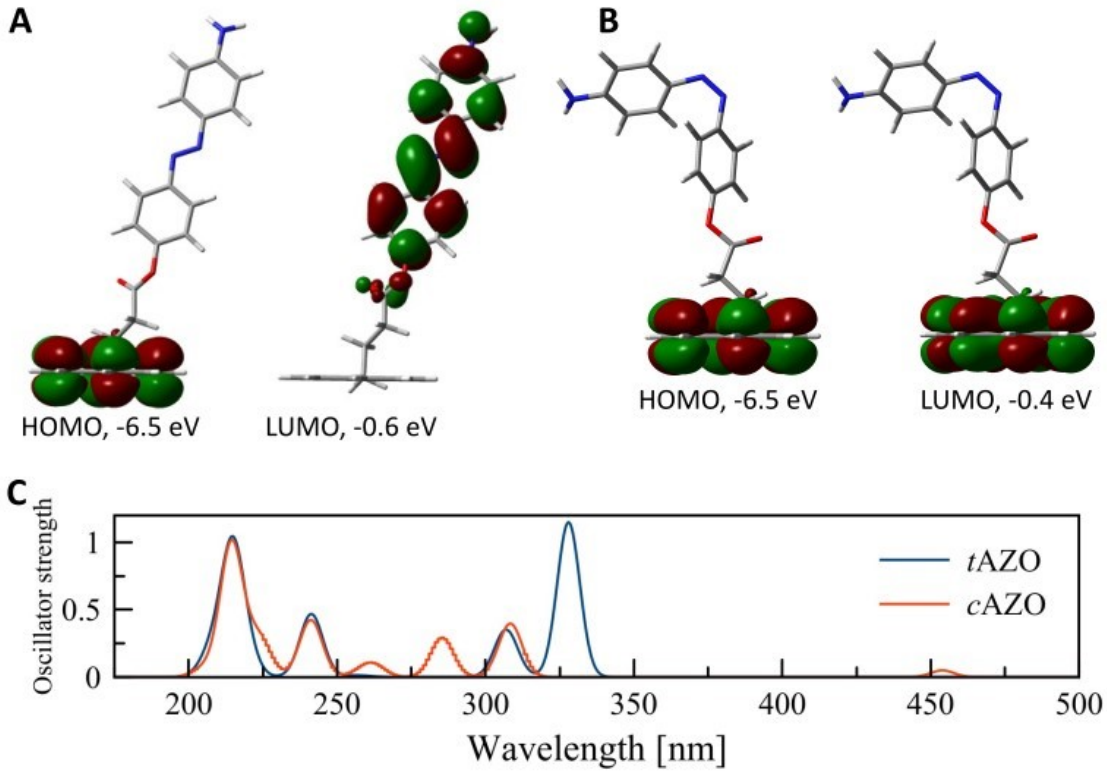


**Figure S2** Frontier orbitals of isolated AZO molecules (A – *trans*, B – *cis*), C - UV-Vis spectra for isolated AZO molecules.

The opening of the conformation lowers the energies of the frontier orbitals, with HOMO at -6.5 eV and LUMO at -0.6 eV for *t*AZO and -0.4 eV for *c*AZO, which leads to energy gap of 5.9 eV and 6.1 eV, respectively. For *t*AZO HOMO is localized on pyrene, whereas LUMO is located on AZO, which suggests a possible intramolecular charge transfer upon excitation (Figure S1A). Both frontier orbitals for *c*AZO in the open conformation are localized on the pyrene moiety, which suggest limitations in charge transfer ability for this isomer (Figure S1B). For *t*AZO the first excited state is a forbidden n→π* transition (HOMO-3 to LUMO), therefore is not visible on the spectra (see Table S1). The first bright peak is at 328 nm, which is related to the second excited state ($S_2$) and corresponds to a HOMO-1 to LUMO transition (π →π*). The next peak at 306 nm corresponds to HOMO to LUMO+1 transition. For the *c*AZO isomer, similar absorption peaks are obtained compared to the *t*AZO, albeit blue shifted by 20 nm. In addition, now the first excited state is weakly allowed and it shows as a peak at 454 nm, which corresponds to n→π* (HOMO-1 to LUMO+1) transition. The next peak at 309 nm corresponds to a HOMO to LUMO transition.

From a geometrical point of view, all three processes require less energy for *t*AZO than for *c*AZO. For PET and PHT the amount of energy required for geometrical changes is similar and nearly twice as high for *c*AZO compared to *t*AZO. Considerably lower $\lambda$ is observed for EET, with the value of only 0.14 eV for *t*AZO and 0.24 eV for *c*AZO, suggesting that (similar to fold conformation) this process might be favored.

The coupling for *t*AZO in open conformation favors the EET process between almost degenerated pyrene excitations at 308 nm and 306 nm and AZO excitation at 328 nm. The EET coupling for this molecule (21.3 meV) is one magnitude higher than the coupling for both charge transfers. Quite low couplings for all three processes are calculated for *c*AZO in the open conformation and it seems that for this molecule EET (between $D^*_{PYR}$ at 309 nm and $A^*_{AZO}$ at 454 nm) and PET (between $D^*_{PYR}$ at 309 nm and $D_{PYR}{\rightarrow}A_{AZO}$ at 263 nm) can be competitive processes.

**Dominant transitions for the isolated molecule**

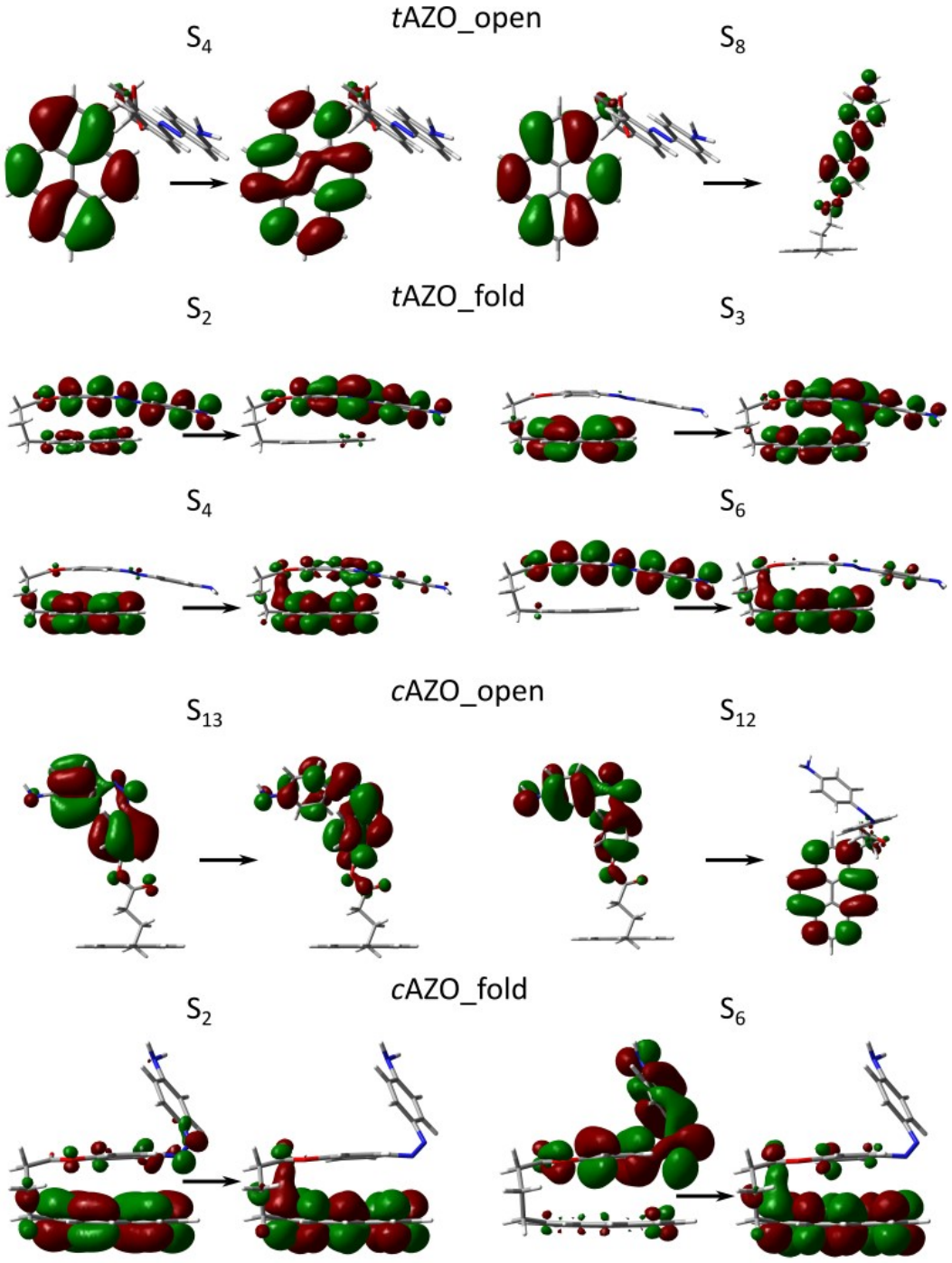


**Figure S3** NTOs of AZO's excites states.

**Geometrical displacements**

| | tAZO | tAZO (top) | cAZO | cAZO (top) |
|---|---|---|---|---|

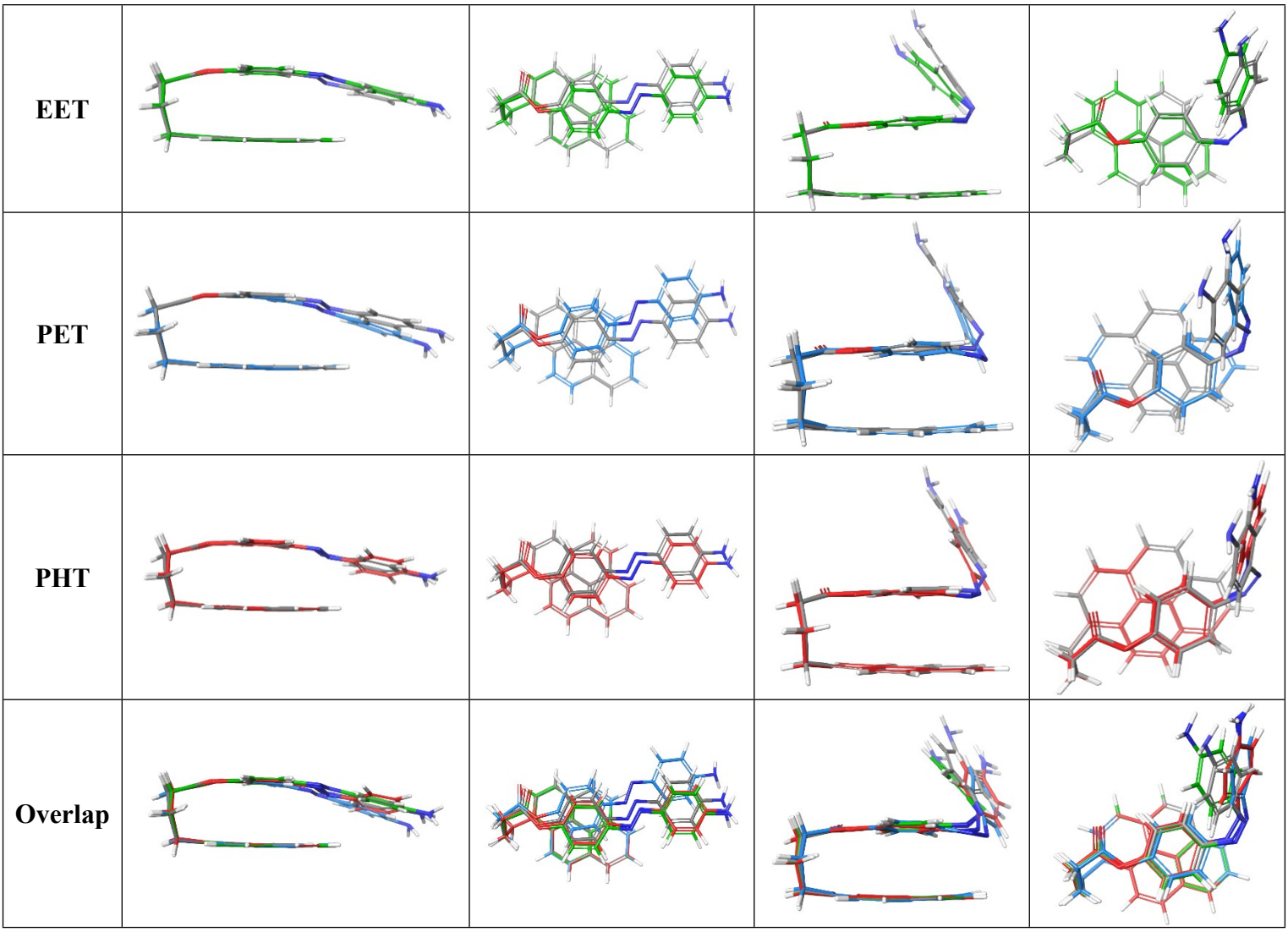


**Figure S4** Geometrical differences for the optimized tAZO and cAZO structures for the three considered processes. Gray: structure in the ground state geometry; green: structure in the excited state, blue: structure with one additional electron; red: structure with one additional hole. The overlap among PHT, PET and EET is also reported.

**Density of states analysis for the GQD-AZO interfaces**

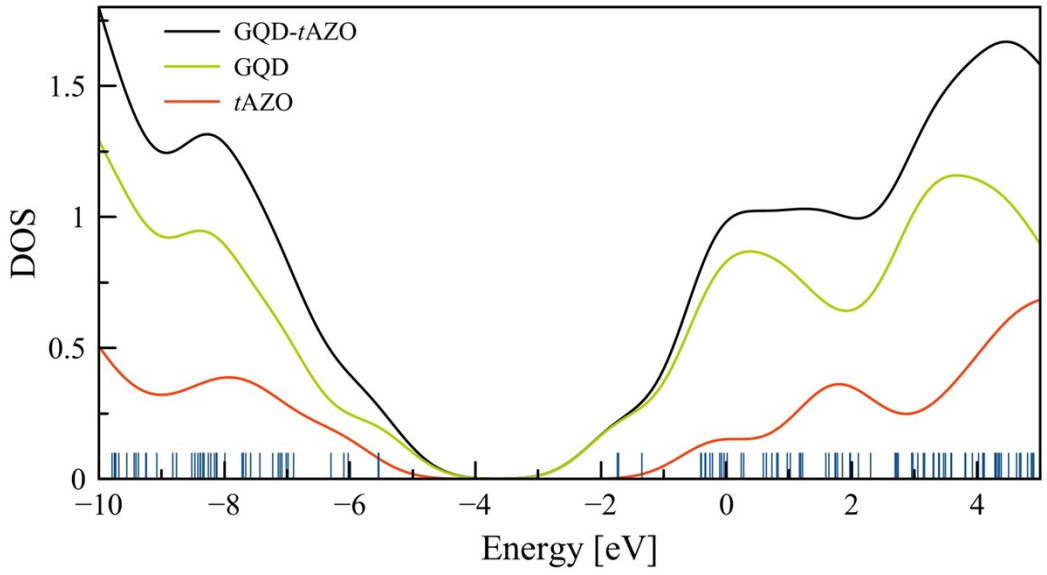


**Figure S5** Density of states for GQD-*t*AZO as well as partial DOS for GQD and *t*AZO.

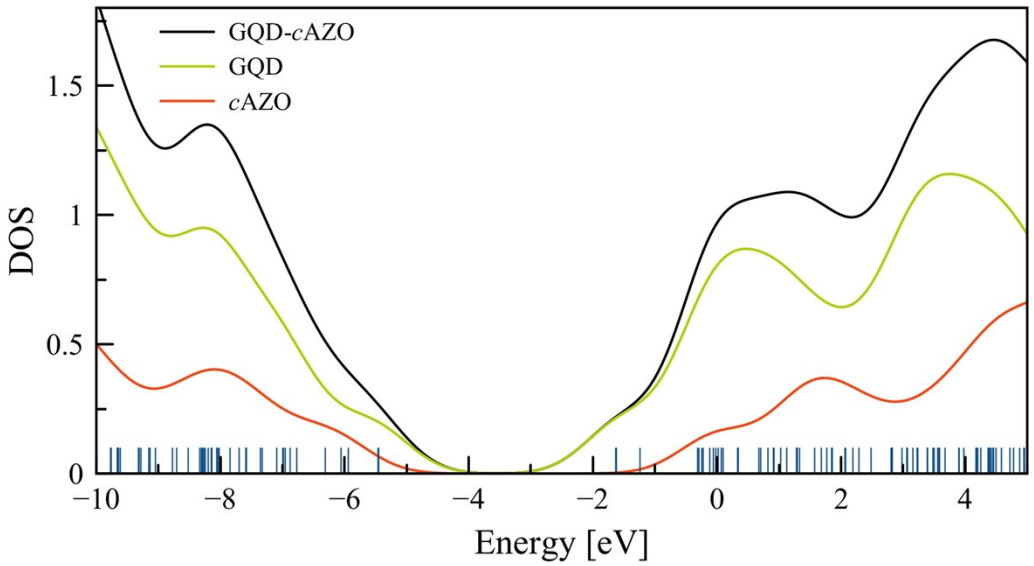


**Figure S6** Density of states for GQD-*c*AZO as well as partial DOS for GQD and *c*AZO.

**Energy level alignment at the GQD-AZO interfaces**

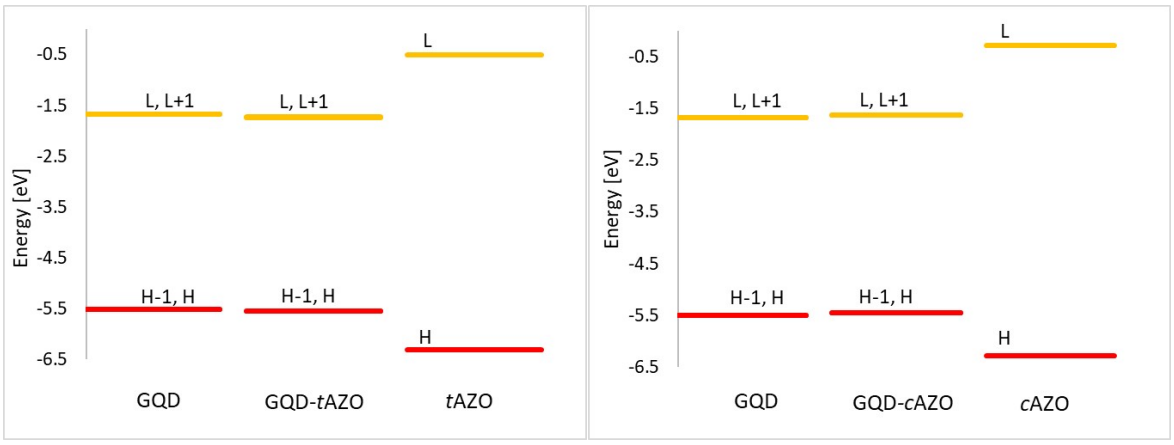


**Figure S7** The alignment of frontier orbitals' energies for GQD, AZO and GQD-AZO for GQD-*t*AZO (left) and GQD-*c*AZO (right).

**Dominant transitions for the interfaces**

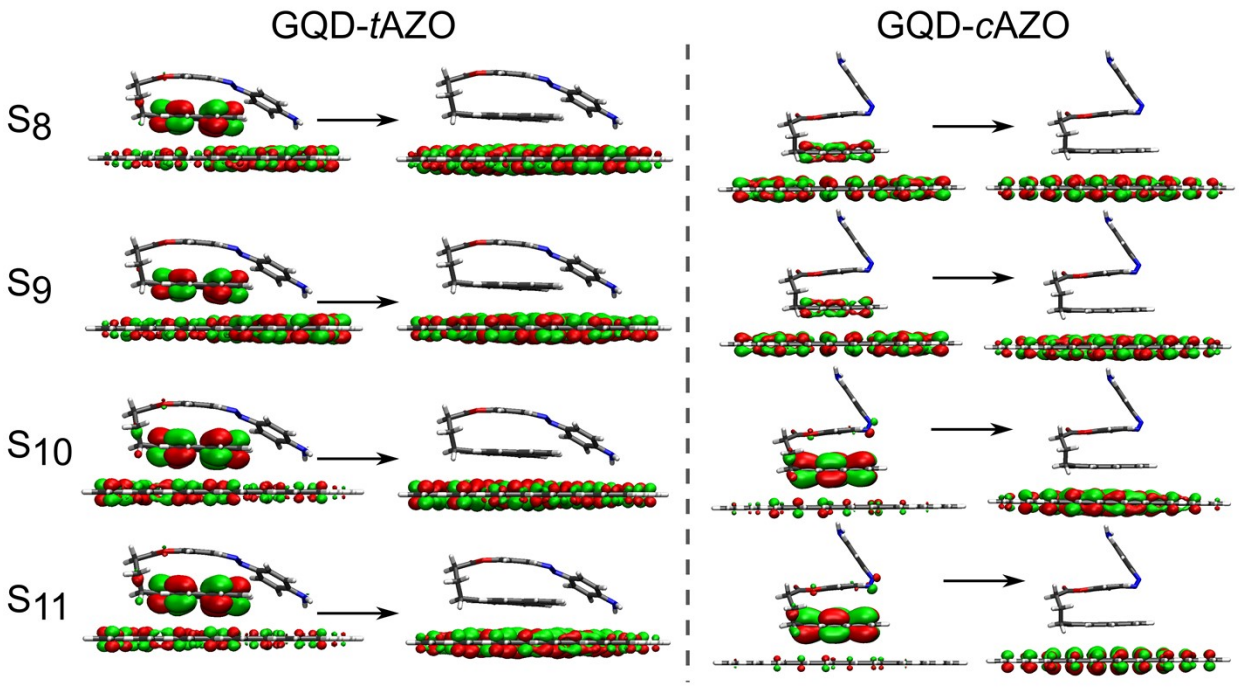


**Figure S8** Natural transition orbitals for excited states that take part in PHT for GQD-tAZO (left) and GQD-cAZO (right).

**Geometry of the assemblies**

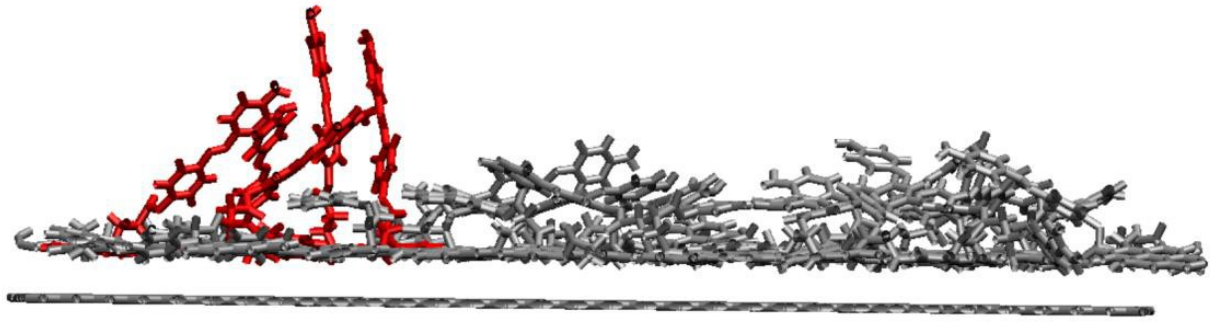

**Figure S9** The final geometry of the interface composed of graphene and 42 *c*AZO molecules. Red molecules resemble open conformation of *c*AZO.

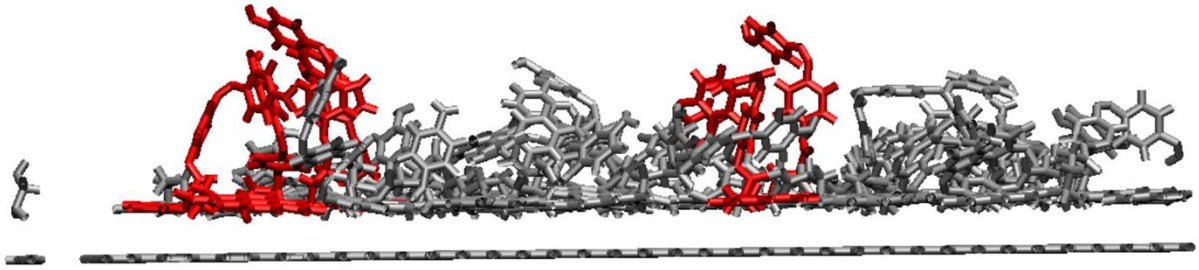

**Figure S10** The final geometry of the interface composed of graphene and 42 *t*AZO molecules. Red molecules resemble open conformation of *t*AZO.

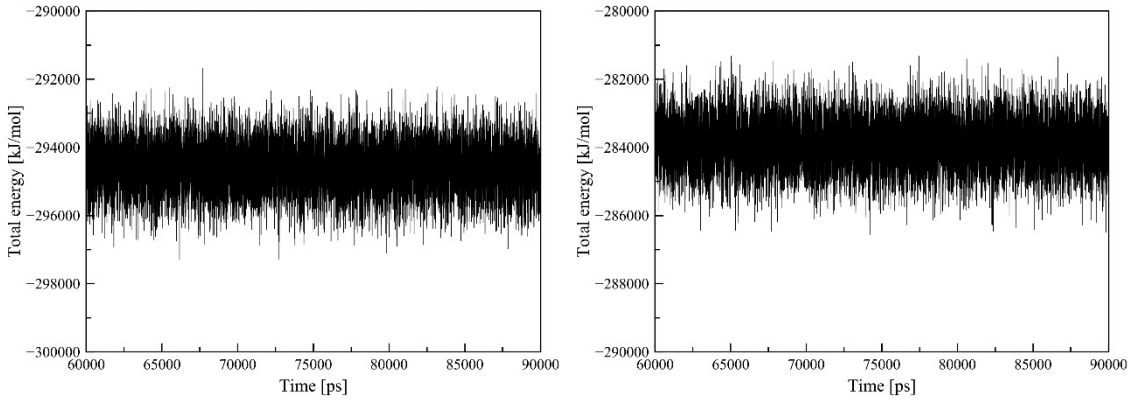


**Figure S11** Total energy equilibration during MD for SLG-*t*AZO (left) and SLG-*c*AZO (right).

**Photophysical properties for the interfaces from MD simulations**

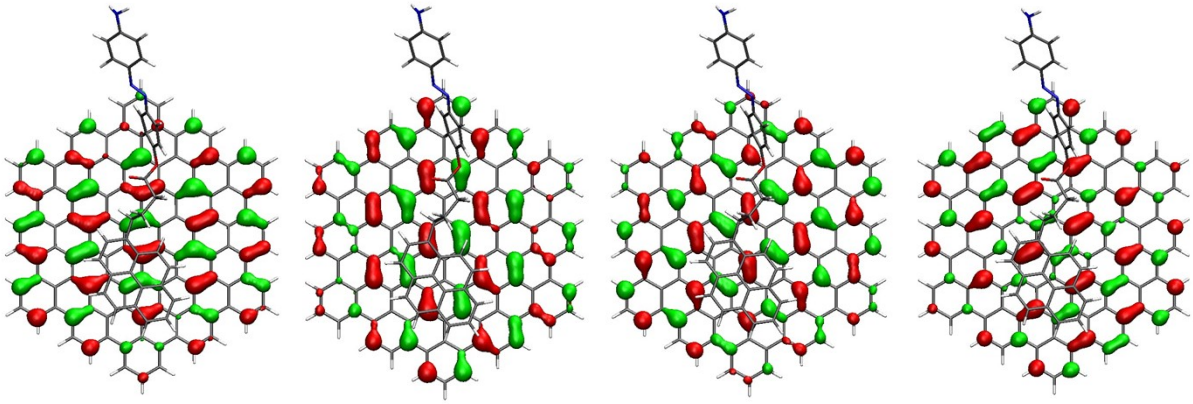

**Figure S12** The visualization of FMOs for the first MD frame.

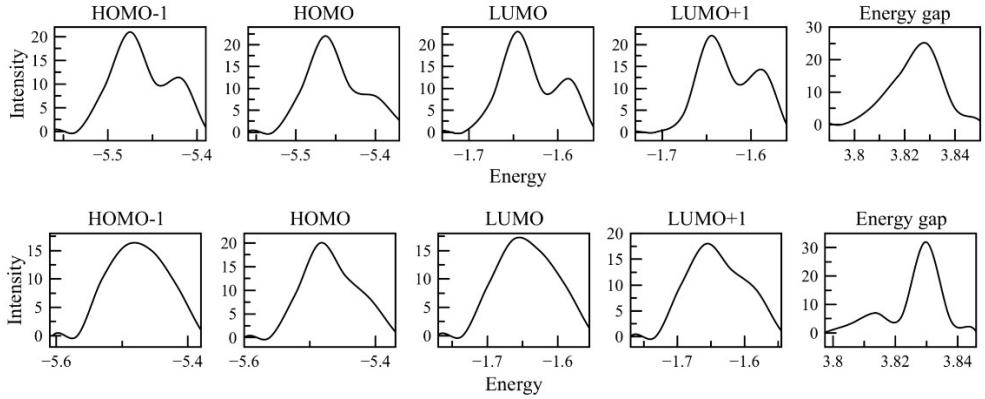


**Figure S13** Distribution of FMOs' energy for the extracted frames.

**Table S3.** Coupling analysis for the different interfaces.

| Model | Process's type | Involved transitions | Coupling [meV] |
|---|---|---|---|
| *t*AZO_fold | EET | $D^*_{PYR}$ ($S_4$), $A^*_{AZO}$ ($S_2$) | 46.4 |
| | PET | $D^*_{PYR}$ ($S_4$), $D_{PYR}\rightarrow A_{AZO}$ ($S_3$) | 44.9 |
| | PHT | $A^*_{AZO}$ ($S_2$), $A_{AZO}\rightarrow D_{PYR}$ ($S_3$) | 64.3 |
| *c*AZO_fold | EET | $D^*_{PYR}$ ($S_2$, $S_3$), $A^*_{AZO}$ ($S_4$) | 9.0 |
| | PET | $D^*_{PYR}$ ($S_2$, $S_3$), $D_{PYR}\rightarrow A_{AZO}$ ($S_{11}$) | 8.9 |
| | PHT | $A^*_{AZO}$ ($S_4$), $A_{AZO}\rightarrow D_{PYR}$ ($S_{11}$) | 105.5 |
| GQD-*t*AZO | EET | $D^*_{AZO}$ ($S_7$), $A^*_{GQD}$ ($S_3$, $S_4$) | 5.3 |
| | PET | $D^*_{AZO}$ ($S_7$), $D_{AZO}\rightarrow A_{GQD}$ ($S_{10}$, $S_{11}$) | 0.5 |
| | PHT | $A^*_{GQD}$ ($S_8$, $S_9$), $A_{GQD}\rightarrow D_{AZO}$ ($S_{10}$, $S_{11}$) | 51.2 |
| GQD-*c*AZO | EET | $D^*_{AZO}$ ($S_3$), $A^*_{GQD}$ ($S_4$, $S_5$) | 10.3 |
| | PET | $D^*_{AZO}$ ($S_3$), $D_{AZO}\rightarrow A_{GQD}$ ($S_{10}$, $S_{11}$) | 4.3 |
| | PHT | $A^*_{GQD}$ ($S_8$, $S_9$), $A_{GQD}\rightarrow D_{AZO}$ ($S_{10}$, $S_{11}$) | 70.4 |
| GQD-*t*AZO_MD | EET | $D^*_{AZO}$ ($S_7$), $A^*_{GQD}$ ($S_3$, $S_4$) | 2.1 |
| | PET | $D^*_{AZO}$ ($S_7$), $D_{AZO}\rightarrow A_{GQD}$ ($S_{10}$, $S_{11}$) | 0.2 |
| | PHT | $A^*_{GQD}$ ($S_8$, $S_9$), $A_{GQD}\rightarrow D_{AZO}$ ($S_{10}$, $S_{11}$) | 41.5 |
| GQD-*c*AZO_MD | EET | $D^*_{AZO}$ ($S_3$), $A^*_{GQD}$ ($S_4$, $S_5$) | 6.9 |
| | PET | $D^*_{AZO}$ ($S_3$), $D_{AZO}\rightarrow A_{GQD}$ ($S_{10}$, $S_{11}$) | 0.5 |
| | PHT | $A^*_{GQD}$ ($S_8$, $S_9$), $A_{GQD}\rightarrow D_{AZO}$ ($S_{10}$, $S_{11}$) | 24.8 |

## References


[1] Cupellini, L., Corbella, M., Mennucci, B. & Curutchet, C. Electronic energy transfer in biomacromolecules. *WIREs Comput. Mol. Sci.* **9**, 1–23 (2019)

[2] Cupellini, L., Giannini, S., Mennucci, B. Electron and excitation energy transfers in covalently linked donor-acceptor dyads: mechanisms and dynamics revealed using quantum chemistry. *Phys. Chem. Chem. Phys.* **20**, 395–403 (2018).

[3] Nottoli, M. et al. The role of charge-transfer states in the spectral tuning of antenna complexes of purple bacteria. *Photosynth. Res.* **137**, 215–226 (2018).

[4] Tölle, J., Cupellini, L., Mennucci, B., Neugebauer, J. Electronic couplings for photo-induced processes from subsystem time-dependent density-functional theory: the role of the diabatization. *J. Chem. Phys.* **153**, 184113 (2020).